Available online at www.sciencedirect.com
ScienceDirect
Materials Research Bulletin 43 (2008) 539–545
Materials Research Bulletin
www.elsevier.com/locate/matresbu

Synthesis of highly dispersed $MnCeO_x$ catalysts *via* a novel ''redox-precipitation'' route

Francesco Arena [a,b,*], Giuseppe Trunfio [a], Jacopo Negro [a], Lorenzo Spadaro [b]

[a] *Dipartimento di Chimica Industriale e Ingegneria dei Materiali, Università degli Studi di Messina, Salita Sperone 31 c.p. 29, I-98166 S. Agata, Messina, Italy*
[b] *Istituto CNR-ITAE ''Nicola Giordano'', Salita S. Lucia 39, I-98126 S. Lucia, Messina, Italy*

Received 8 November 2006; received in revised form 7 February 2007; accepted 3 May 2007
Available online 6 May 2007

Abstract

A new synthesis route driving redox-precipitation reactions among Mn^{VII}, Ce^{III} and Mn^{II} precursors in basic aqueous solution yields $MnCeO_x$ catalysts (Mn loading, 9–33 wt%) with improved textural and structural properties in comparison to the conventional co-precipitation technique. Irrespective of the Mn loading, BET, X-ray diffraction (XRD), transmission electron microscopy (TEM) and X-ray photoelectron spectroscopy (XPS) findings prove that the new method ensures a very high reproducibility in all the main physico-chemical properties of $MnCeO_x$ catalysts. Enabling a *monolayer dispersion* of the active phase, the ''redox-precipitation'' method greatly promotes the reducibility and the *surface affinity* of the $MnCeO_x$ system towards gas-phase oxygen.

Keywords: A. Oxides; A. Nanostructures; B. Chemical synthesis; D. Crystal structure; D. Surface properties

1. Introduction

Environmental catalysis is a rapidly growing field of both academic and technological interest pressed by the urgent need to preserve natural resources and human health. On this account a variety of catalytic processes for removing noxious organic pollutants in both gas-exhausts and wastewaters, mostly based on total oxidation reactions, are actually under scrutiny worldwide.

Although uncommon targets and reaction conditions do not allow assessing general rules on environmental catalysts requirements yet, according to theoretic principles of oxidation catalysis [1,2], an easy mobility and availability of oxygen at the catalyst surface constitutes the necessary condition for an effective conversion of organic substrates into carbon dioxide.

Potential alternative to high-cost noble-metal catalysts commonly employed in total oxidation processes [1–5], the $MnCeO_x$ system has attracted, since several decades, a great deal of research interest due to its noticeable performance in the catalytic wet oxidation of wastewaters with oxygen (CWO) [3–12], the catalytic combustion of VOC's [13–20] and the conversion/decomposition of NO_x [21,22]. A superior catalytic activity is generally associated with an enhanced ''reducibility'' of ''highly dispersed'' manganese ions [4–13,16,20–23], while the reversibility of the redox

* Corresponding author at: Dipartimento di Chimica Industriale e Ingegneria dei Materiali, Università degli Studi di Messina, Salita Sperone 31 c.p. 29, I-98166 S. Agata, Messina, Italy. Tel.: +39 090 6765606; fax: +39 090 391518.
E-mail address: Francesco.Arena@unime.it (F. Arena).

0025-5408/$ – see front matter
doi:10.1016/j.materresbull.2007.05.007

cycle involving surface manganese/ceria ions is critical for catalyst stability [6–9,14]. A proper "tuning" of textural, structural, and electronic features of the active phase has been then indicated as a benchmark for improving the reactivity of $MnCeO_x$ systems [4–11,20–23].

Therefore, this paper is aimed at probing that an original synthesis route driving *redox-precipitation* reactions among Mn and Ce precursors in basic solution leads to *monolayer-dispersed* $MnCeO_x$ catalysts in a very wide range (9–33 wt%) of the manganese loading. With a very high reproducibility, the redox-precipitation method allows improving the physico-chemical properties and the redox pattern of $MnCeO_x$ catalysts in comparison to the conventional co-precipitation technique.

2. Experimental

2.1. Catalysts

$MnCeO_x$ catalysts with different Mn-to-Ce atomic ratio (Mn_{at}/Ce_{at}, 0.33–2.1) were prepared *via* the novel "*redox-precipitation*" route, according to the following procedure. An amount of the $KMnO_4$ precursor in deionized water was titrated at ca. 333 K under vigorous stirring with an aqueous solution containing both $Ce(NO_3)_3$ and $Mn(NO_3)_2$ precursors. Keeping constant pH (8.0 ± 0.3) by the addition of a 0.2 M KOH solution, it has been ascertained that the following redox reactions:

$$MnO_4^- + 3e^- + 2H_2O \rightarrow MnO_2 \Downarrow + 4HO^- \quad (1)$$

$$Mn^{2+} + 4HO^- \rightarrow MnO_2 \Downarrow + 2e^- + 2H_2O \quad (2)$$

$$Ce^{3+} + 4HO^- \rightarrow CeO_2 \Downarrow + e^- + 2H_2O \quad (3)$$

occur in a quantitative way. With a lower limit of the Mn_{at}/Ce_{at} ratio equal to 0.33 (e.g., $mol_{Mn}^{II} = 0$), the designed catalyst composition was obtained dosing the various precursors according to the following quantitative relationships

$$3\,mol_{Mn^{VII}} = 2\,mol_{Mn^{II}} + mol_{Ce^{III}} \quad (a)$$

$$\frac{mol_{Mn^{VII}} + mol_{Mn^{II}}}{mol_{Ce^{III}}} = \left(\frac{Mn_{at}}{Ce_{at}}\right)_{design} \quad (b)$$

$$mol_{Mn^{VII}} + mol_{Mn^{II}} + mol_{Ce^{III}} = 1, \quad (c)$$

referred to electron (a) and mass (c) balance and catalyst composition (b), respectively. After titration, the solid was further digested for 30 min and then filtered, repeatedly washed with hot distilled water and dried overnight at 373 K. Aliquots of the dried samples were further calcined in air at 673 K (6 h).

A reference $MnCeO_x$ catalysts (Mn_{at}/Ce_{at}, 1.0) was prepared by the co-precipitation route using $MnCl_2$ and $CeCl_3$ (M1C1-P4) precursors and a 10 wt% Na_2CO_3 solution as precipitant [6–10,14,23]. After precipitation, the solid was dried at 373 K and then calcined in air at 673 K (6 h).

The list of the studied samples with the relative physico-chemical properties is given in Table 1.

Table 1
List of the studied catalysts

Catalyst	Mn_{at}/Ce_{at} [a]		[Mn] (wt%)	Preparation method	SA_{BET} (m^2/g)	P.V. (cm^3/g)	A.P.D. [b] (Å)
	Des.	Exp.					
M1C3-R4	0.33	0.33	9.0	Redox-precipitation	148	0.25	54
M3C4-R4	0.75	0.71	16.7	Redox-precipitation	169	0.40	95
M1C1-R4	1.00	0.95	20.5	Redox-precipitation	154	0.44	111
M3C2-R4	1.50	1.44	26.7	Redox-precipitation	157	0.39	99
M2C1-R4	2.00	2.13	32.8	Redox-precipitation	150	0.46	131
M1C1-P4	1.00	0.94	20.4	Co-precipitation	101	0.24	94

[a] Atomic ratio from design and XRF analysis, respectively.
[b] Average pore diameter (4 P.V./SA_{BET}).

2.2. Surface area (SA_{BET}) and pore size distribution (PSD)

Surface area (SA_{BET}) and pore size distribution data were obtained from the nitrogen absorption/desorption isotherms at 77 K which were elaborated according to the BET method for the calculation of surface area.

2.3. X-ray diffraction (XRD)

X-ray diffraction analysis of powdered samples was performed in the 2θ range 20–75° using a Philips X-Pert diffractometer operating with a Ni β-filtered Cu Kα radiation at 40 kV and 30 mA. The ceria average particle size was calculated by the Sherrer's equation.

2.4. Transmission electron microscopy (TEM)

Transmission electron microscopy analysis of the catalysts was performed using a PHILIPS CM12 Microscope (point-to-point resolution, 3 Å).

2.5. X-ray photoelectron spectroscopy (XPS)

X-ray photoelectron spectroscopy data were obtained by a Physical Electronics GMBH PHI 5800-01 spectrometer, using a monochromatized Al Kα radiation with a power beam of 350 W and a pass energy of 60 eV. The studied BE regions were 635–680 eV (Mn_{2p}), 280–300 eV (C_{1s}), 525–540 eV (O_{1s}) and 870–935 eV (Ce_{3d}), using the C_{1s} line (284.8 eV) of *adventitious carbon* as reference.

2.6. Temperature programmed reduction (TPR)

Temperature programmed reduction measurements in the range 273–1073 K were performed using a 6% H_2/Ar mixture flowing at 60 stp mL min^{-1} into a linear microreactor (d_{int}, 4 mm) containing a catalysts sample of ca. 30 mg heated at the rate of 12 K min^{-1}. Measurements were performed without any pretreatment of the ''as prepared'' samples and after a pretreatment *in situ* at 673 K for 30 min in an oxygen flow (30 stp mL min^{-1}).

3. Results and discussion

3.1. Structural and morphological properties

The purpose of maximizing the dispersion of the active phase for improving the oxidizing strength and the reactivity of the $MnCeO_x$ system in the CWO process [4–13], pressed the design of a novel synthesis route to attain a mixture of the oxide components at an *atomic level*. Since the limitation of the conventional co-precipitation technique, consisting in the formation of ''monophasic'' solid particles because of the different precipitation kinetics of each cation [23], a selective ''cogeneration'' of the MnO_2 and CeO_2 phases by redox interactions among proper precursors has been exploited.

A preliminary evidence of the peculiar structural features induced by the novel synthesis route stems from a much larger surface exposure of redox-precipitated catalysts (150–170 m^2/g) in comparison to the co-precipitated system (101 m^2/g). Moreover, in spite of a widely changing chemical composition (Table 1), the method ensures a very high reproducibility of the solid texture, this being a peculiar feature of the redox-precipitation route [5–10,18–23].

The XRD data of the studied systems, shown in Fig. 1A, confirm the peculiarity of the new synthesis route, also in terms of structural characteristics of the $MnCeO_x$ system. The co-precipitated catalyst displays a conventional pattern characterized by the typical diffraction lines of the cerianite with the fluorite-like structure, along with poorly resolved reflexes at 37.3° and 42.4°, diagnostic of an incipient crystallization of manganese oxide in the form of *pyrolusite* [6–8,16,17,27]. Whereas, irrespective of the composition, fairly atypical diffraction patterns featuring a main broad signal spanned in the 2θ range 20–40° and another less component between 40° and 60° (Fig. 1A), are recorded for redox-precipitated samples. An intensity regularly decreasing with the Mn_{at}/Ce_{at} ratio suggests that these components are related to the ceria matrix, as further confirmed by the XRD data of the M1C1-R4 sample calcined at 873 and 1073 K

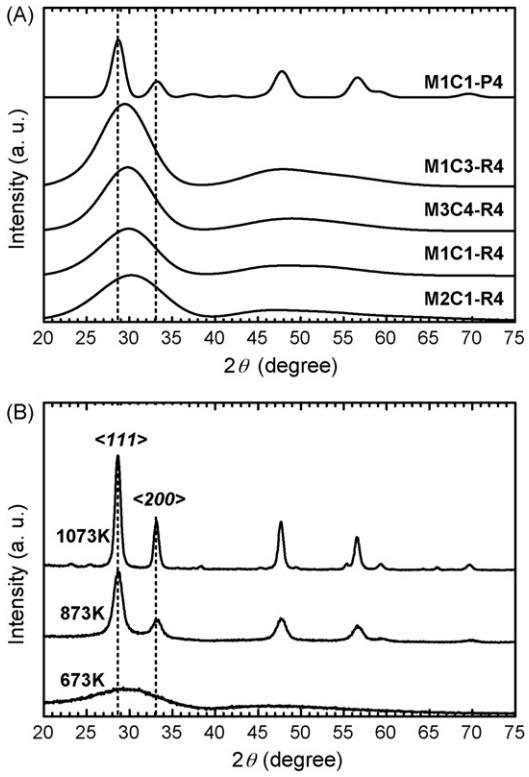

Fig. 1. (A) Influence of preparation method and Mn loading on the XRD pattern of $MnCeO_x$ catalysts. (B) Effect of the calcination temperature (673, 873, 1073 K) on the XRD pattern of the M1C1-R sample.

(Fig. 1B), outlining in the 20–40° range only the lines relative to the ⟨1 1 1⟩ and ⟨2 0 0⟩ faces of the cerianite [6–9,13–16,22–24]. Therefore, these diffraction patterns are diagnostic of the lack of a *"long-range"* crystalline order which, according to the characteristics of the synthesis route, can be attributed to a very intimate *sticking* of MnO_x and CeO_x molecules hindering the growth of "large" crystalline domains. Indeed, similar diffractograms were recorded for highly dispersed ceria systems with a particle size in the order of few (e.g., 1–2 nm) nanometers, characterized by a surface-to-total cerium ions ratio close to 100% [14,24–26].

By contrast, the inability of the co-precipitation technique to get a very intimate mix of the oxides [23] is confirmed by the presence of crystalline MnO_2 and CeO_2 phases on the M1C1-P4 sample (Fig. 1A). In agreement with the surface exposure (Table 1), a mean ceria particle size of ca. 55 Å is indeed calculated for this system [5–10,23].

TEM pictures of the representative M1C1-P4 (A and B) and M1C1-R4 (C and D) catalysts (Fig. 2) support previous experimental evidences on the different structural features of co-precipitated and redox-precipitated systems. The M1C1-P4 system consists of large and "closely packed" agglomerates of "stepped" particles (5–10 nm) with an irregular morphology (Fig. 2A). At high magnification (Fig. 2B), the specimen appears as an intricate array of randomly and "stepped" crystalline domains (5–10 nm), characterized by the presence of ordered fringes with an estimated inter-atomic distance of 3.2 Å typical of crystalline ceria [25]. Although the morphology of the aggregates is not too much dissimilar from that of the co-precipitated sample, the M1C1-R4 sample looks much less densely "packed" (Fig. 2C) while, a sporadic presence of small crystalline (3–5 nm) domains, randomly dispersed into a prevalently "amorphous" matrix, renders poorly evident ceria domains at high magnification (Fig. 2D). With a surface Mn/Ce ratio close to the nominal bulk composition (1.0 ± 0.2), EDX analysis (circled areas) signals a rather uniform chemical composition of the last sample at any level, while a much larger range of variation (0.2–6) in the surface Mn/Ce atomic ratio confirms the presence of relatively large and "chemically homogeneous" CeO_2 and MnO_x domains on the M1C1-P4 catalyst.

Further, XPS analysis has been carried out to shed lights into the effects of preparation method and manganese loading on the surface atomic composition and dispersion of the active phase. In particular, to assess the relative

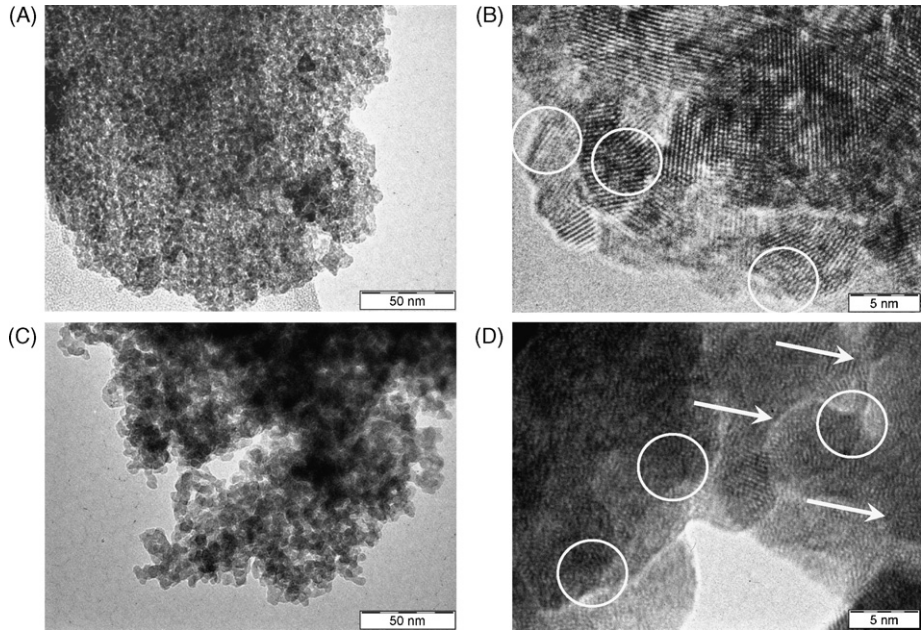

Fig. 2. TEM micrographs of the M1C1-P4 (A and B) and M1C1-R4 (C and D) catalysts.

distribution of the active phase across the ceria matrix, the XPS data of the redox-precipitated catalysts are plotted as surface Mn/Ce atomic ratio (e.g., Mn_{2p}/Ce_{3d}) against the bulk composition (Table 1) in Fig. 3. A very accurate straight-line correlation starting from the origin denotes a constant degree of dispersion of manganese oxide across the ceria matrix and, though a slope value (1.26) larger than one could signal some surface segregation of the active phase, this finding is virtually consistent with a *monolayer dispersion* of the active phase irrespective of the loading, this being a further remarkable characteristic of the new synthesis route. On the other hand, with a Mn/Ce surface value (0.42) three-fold lower than that of the counterpart M1C1-R4 sample (Fig. 3), surface analysis data confirm a much lower dispersion of the active phase on the co-precipitated system.

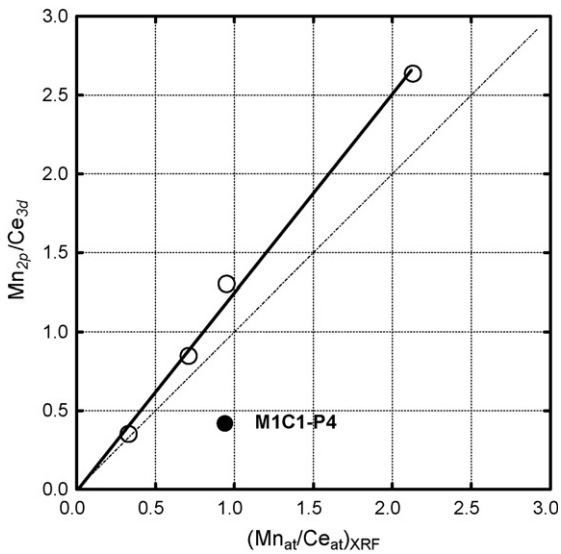

Fig. 3. Surface manganese-to-cerium atomic ratio (from Mn_{2p} and Ce_{3d} XPS signals) vs. the bulk composition (see Table 1) of redox-precipitated catalysts. For reference the Mn_{2p}/Ce_{3d} XPS ratio of the "co-precipitated" (●) sample is shown.

Therefore, the basic information of structural characterization findings is that in redox-precipitated samples the MnO_x and CeO_2 phases are mixed at (quasi)atomic level, forming an amorphous background ''embedding'' a small concentration of *nanosized* ceria domains.

3.2. Redox properties

According to literature findings indicating some close relationships among dispersion, manganese A.O.N. and catalyst reducibility [4,6–8,11–13,21], the TPR profiles of the ''untreated'' (A) and ''pretreated'' (B) M1C1-R4 and M1C1-P4 catalysts (Fig. 4) display a redox behavior strongly related to the preparation method. Considering two different regions of hydrogen consumption, relative to the reduction of the active phase (LTR, 273–723 K) and ceria carrier (HTR, 723 K–1073) [5–7,10–12,16,20] respectively, a marked influence of the preparation method on the redox behavior of the system is also evident, both in qualitative and quantitative terms. The profile of the ''untreated'' M1C1-P4 system (Fig. 4A) consists of two resolved peaks in the LTR centered at 600 and 688 K with an onset temperature of reduction ($T_{o,red}$) of 400 K, along with a quite smaller band of H_2 consumption with the maximum at ca. 990 K (HTR), monitoring the reduction of sub-surface Ce^{4+} ions [5–7,10,11,16,20,27]. The total hydrogen consumption equals to ca. 3.3 mmol/g, while that in LTR (2.65 mmol/g) accounts for a H_2/Mn ratio equal to 0.70. Visibly shifted to lower temperature ($T_{o,red}$, 365 K), the reduction profile of the M1C1-R4 system in the LTR shows a ''narrower'' band of hydrogen consumption with two close and poorly resolved maxima at 545 and 591 K, while a slighter ceria reduction peak is observed in the HTR. Overall, a hydrogen consumption of 3.60 mmol/g accounts for a larger H_2/Mn ratio (0.85), consistent with a higher MnO_x dispersion [6–8,10,12,27]. Indeed, the latter catalyst misses the component at ca. 670 K relative to crystalline MnO_x particles [15,27] while, associated with the reduction of ''isolated'' Mn^{4+} ions, the peak at 545 K is nearly absent in the spectrum of the co-precipitated system as the much lower dispersion of the active phase.

An oxidative pretreatment (673 K) stresses further the differences in the redox behavior of the two systems (Fig. 4B). The TPR profile of the co-precipitated sample displays in fact (see the difference profile) only a slightly larger intensity of reduction peaks in the LTR, accounting for a moderate increase (0.81) of the H_2/Mn ratio. The M1C1-R4 sample is characterized instead by a much higher rate of H_2 consumption in the LTR, evidenced by the appearance of a new component (T_M, 422 K) in the range 323–423 K lowering the onset temperature of reduction (290 K) by ca. 100 K with respect to the untreated sample. The new component, adding to a (slightly) larger intensity of the other peaks (see difference profile), results in a marked increase of the H_2/Mn ratio (1.06). Therefore, such

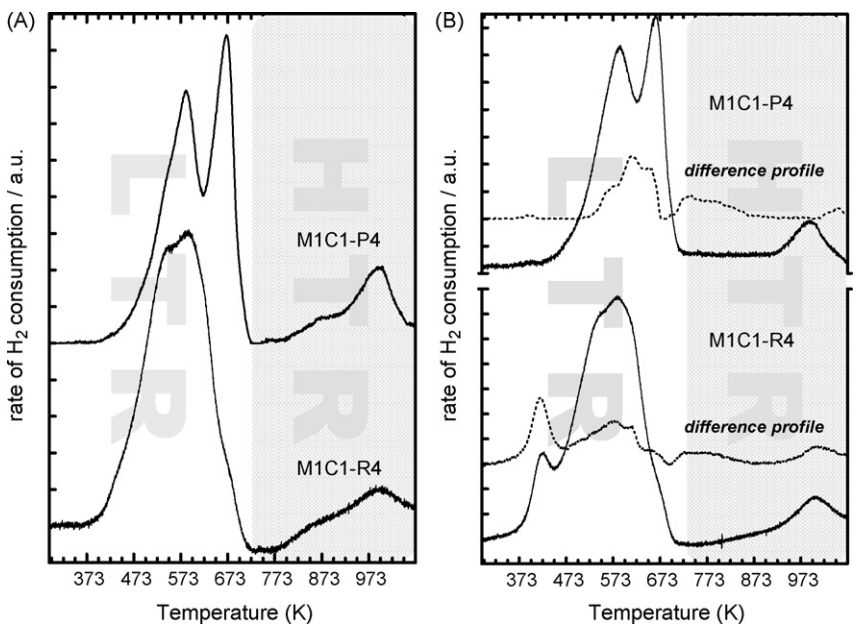

Fig. 4. TPR profiles of the M1C1-R4 and M1C1-P4 catalysts: (A) ''untreated'' and (B) pre-treated *in situ* in oxygen flow at 673 K (30 min).

findings signal an improved oxygen availability due to a very different affinity of systems towards gas-phase oxygen. In fact, this can be explained considering that the removal of water molecules from the first coordinative shell of highly unsaturated ''isolated'' Mn^{4+} ions during the oxidative treatment prompts the adsorption and activation of molecular oxygen, which allows for the stabilization of very reactive *electrophylic* oxygen species at the catalyst surface [1,2]. Noteworthy, these oxygen species would markedly enhance the *oxidizing strength* and the total oxidation capacity of the system in a temperature range suitable for many catalytic applications [1–22]. While, this effect is negligible for the co-precipitated system owing to two concomitant negative effects linked to a much lower dispersion of the active phase. Namely, a low surface availability of manganese ions in crystalline MnO_x particles and a consequent lower degree of coordinative unsaturation concur to depress the affinity of the co-precipitated system towards gas-phase oxygen.

4. Conclusions

A new synthesis route driving redox-precipitation reactions among various Mn and Ce precursors leads to *highly dispersed* $MnCeO_x$ catalysts.

Irrespective of the manganese loading (9–33 wt%), the *redox-precipitation* method ensures a *constant larger surface exposure* and a *monolayer dispersion* of the active phase.

Improved structural and textural properties promote the redox behavior and the affinity to gas-phase oxygen of redox-precipitated $MnCeO_x$ catalysts.

The *redox-precipitation* method could open new perspectives in the synthesis of *highly dispersed* materials for catalytic applications.

References

[1] A. Bielañski, J. Haber, Oxygen in Catalysis, Marcel Dekker, Inc., New York, 1991.
[2] V. Sokolovskii, Catal. Rev. -Sci. Eng. 32 (1990) 1.
[3] Y.I. Matatov-Meytal, M. Sheintuch, Ind. Eng. Chem. Res. 37 (1998) 309.
[4] S. Imamura, in: A. Trovarelli (Ed.), Catalysis by Ceria and Related Materials, vol. 14, Imperial College Press, London, UK, 2002, p. 431.
[5] S.K. Bhargava, J. Tardio, J. Prasad, K. Foger, D.B. Akolekar, S.C. Grocott, Ind. Eng. Chem. Res. 45 (2006) 1221.
[6] H. Chen, A. Sayari, A. Adnot, F. Larachi, Appl. Catal. B 32 (2001) 195.
[7] S. Hamoudi, F. Larachi, A. Sayari, J. Catal. 177 (1998) 247.
[8] S.T. Hussain, A. Sayari, F. Larachi, Appl. Catal. B 34 (2001) 1.
[9] M. Abecassis-Wolfovich, R. Jothiramalingam, M.V. Landau, M. Herrskowitz, B. Viswanathan, T.K. Varadarajan, Appl. Catal. B 59 (2005) 91.
[10] F. Arena, J. Negro, A. Parmaliana, L. Spadaro, G. Trunfio, Ind. Eng. Chem. Res. xxx (2007) xxx–xxx.
[11] S.-K. Kim, S.-K. Ihm, Top. Catal. 33 (1–4) (2005) 171.
[12] A.M.T. Silva, R.R.N. Marques, R.M. Quinta-Ferreira, Appl. Catal. B 47 (2004) 269.
[13] D. Terribile, A. Trovarelli, C. de Leitnburg, A. Primavera, G. Dolcetti, Catal. Today 47 (1999) 133.
[14] R. Cracium, Catal. Lett. 55 (1998) 25.
[15] Y. Liu, M. Luo, Z. Whei, Q. Xin, P. Ying, C. Li, Appl. Catal. B 29 (2001) 61.
[16] A. Gil, L.M. Gandía, S.A. Korili, Appl. Catal. A 274 (2004) 229.
[17] W.B. Li, W.B. Chu, M. Zhang, J. Hua, Catal. Today 93–95 (2004) 205.
[18] L. Lamaita, M.A. Peluso, J.E. Sambeth, H.J. Thomas, Appl. Catal. B 61 (2005) 114.
[19] I. Barrio, I. Legórburu, M. Montes, M.I. Domínguez, M.A. Centeno, J.A. Odriozola, Catal. Lett. 101 (3–4) (2005) 151.
[20] X. Tang, Y. Li, X. Huang, Y. Hu, H. Zhu, J. Wang, W. Shen, Appl. Catal. B 62 (2006) 265.
[21] S. Imamura, M. Shono, N. Okamoto, A. Hamada, S. Ispida, Appl. Catal. A 142 (1996) 279.
[22] G. Qi, R.T. Yang, J. Catal. 217 (2003) 434.
[23] G.-Y. Adachi, T. Masui, in: A. Trovarelli (Ed.), Catalysis by Ceria and Related Materials, vol. 3, Imperial College Press, London, UK, 2002 p. 51.
[24] R. Cracium, Solid State Ionics 110 (1998) 87.
[25] X. Zheng, S. Wang, X. Wang, S. Wang, X. Wang, S. Wu, Mater. Lett. 59 (2005) 2769.
[26] S. Tsunekawa, R. Sivamohan, S. Ito, A. Kasuya, T. Fukuda, Nanostruct. Mater. 11 (1999) 141.
[27] F. Arena, T. Torre, C. Raimondo, A. Parmaliana, Phys. Chem. Chem. Phys. 3 (2001) 1911.